Published in final edited form as:
Hum Mutat. 2012 August ; 33(8): 1275–1284. doi:10.1002/humu.22107.

Functional analysis of non-synonymous single nucleotide polymorphisms in human SLC26A9

An-Ping Chen[1], **Min-Hwang Chang**[1], and **Michael F. Romero**[1,2,3,§]

[1]Physiology & Biomedical Engineering, Mayo Clinic College of Medicine, Rochester, MN 55905 USA

[2]Nephrology & Hypertension, Mayo Clinic College of Medicine, Rochester, MN 55905 USA

[3]O'Brien Urology Research Center, Mayo Clinic College of Medicine, Rochester, MN 55905 USA

Abstract

Slc26 anion transporters play crucial roles in transepithelial Cl^- absorption and HCO_3^- secretion; Slc26 protein mutations lead to several diseases. Slc26a9 functions as a Cl^- channel and electrogenic Cl^--HCO_3^- exchanger, and can interact with CFTR. Slc26a9(−/−) mice have reduced gastric acid secretion, yet no human disease is currently associated with SLC26A9 coding mutations. Therefore, we tested the function of non-synonymous, coding, single nucleotide polymorphisms (cSNPs) of *SLC26A9*. Presently, eight cSNPs are NCBI-documented: Y70N, T127N, I384T, R575W, P606L, V622L, V744M and H748R. Using two-electrode voltage-clamp and anion selective electrodes, we measured the biophysical consequences of these cSNPs. Y70N (cytoplasmic N-terminus) displays higher channel activity and enhanced Cl^--HCO_3^- exchange. T127N (transmembrane) results in smaller halide currents but not for SCN^-. V622L (STAS domain) and V744M (STAS adjacent) decreased plasma membrane expression which partially accounts for decreased whole cell currents. Nevertheless, V622L transport is reduced to ~50%. *SLC26A9* polymorphisms lead to several function modifications (increased activity, decreased activity, altered protein expression) which could lead to a spectrum of pathophysiologies. Thus, knowing an individual's *SLC26A9* genetics becomes important for understanding disease potentially caused by SLC26A9 mutations or modifying diseases, e.g., cystic fibrosis. Our results also provide a framework to understand SLC26A9 transport modalities and structure-function relationships.

Keywords

SLC26A9; single nucleotide polymorphisms; voltage clamp; Cl^- channel; intracellular pH; *Xenopus* oocytes

Introduction

Transepithelial chloride absorption and bicarbonate secretion are coupled to fluid secretion and thus important for the normal function of most epithelia. Such coupling is well illustrated in cystic fibrosis tissues in which mutations of cystic fibrosis transmembrane conductance regulator (CFTR, a Cl^- channel) reduce Cl^- and HCO_3^- secretion leading to extracellular dehydration especially in the lung (Riordan, et al., 1989). Similarly, other

§Address correspondence (current address) to: Michael F. Romero, Ph.D., Physiology & Biomedical Engineering, Mayo Clinic College of Medicine, 200 First St SW, Rochester, MN 55905; romero.michael@mayo.edu.

Supporting Information for this preprint is available from the *Human Mutation* editorial office upon request (humu@wiley.com)

diseases such as congenital chloride diarrhea, Pendred syndrome and deafness due to mutations in anion transport of SLC26 family members (Moseley, et al., 1999; Taylor, et al., 2002; Wall, 2006; Wangemann, et al., 2007) also perturb fluid transport.

The human SLC26 transporter family encodes 10 different proteins, and is a part of the "sulfate permease" (i.e. SulP) protein family with homologues in bacteria, plants (Hawkesford, 2003; Takahashi, et al., 1997), fungi (Cherest, et al., 1997; van de Kamp, et al., 2000) and other animals (Dorwart, et al., 2008; Saier, et al., 1999). Slc26 proteins play multiple physiological roles in the transport of several anions, including SO_4^{2-}, Cl^-, I^-, HCO_3^-, SCN^-, OH^-, NO_3^-, formate$^-$ and oxalate^{2-} (Bissig, et al., 1994; Chang, et al., 2009a; Chang, et al., 2009b; Jiang, et al., 2002; Karniski, et al., 1998; Kim, et al., 2005; Moseley, et al., 1999; Mount and Romero, 2004; Satoh, et al., 1998; Scott and Karniski, 2000; Shcheynikov, et al., 2006b; Soleimani, et al., 2001; Xie, et al., 2002). Some Slc26 proteins have tissue-specific expression-patterns while others are widespread (Mount and Romero, 2004). Structurally, these Slc26 proteins assemble as dimers (Detro-Dassen, et al., 2008) with 12 predicted transmembrane spans (Shelden, et al., 2010), and a cytoplasmic COOH-terminus containing a STAS (**S**ulfate **T**ransporter **A**nti-**S**igma) domain (Aravind and Koonin, 2000). Slc26 STAS domains can participate in protein-protein interactions with the R-region of CFTR (Avella, et al., 2011b; Chang, et al., 2009a; Homma, et al., 2010; Ko, et al., 2002; Ko, et al., 2004; Rode, et al., 2012) and also control Slc26 transport function (Everett, et al., 1997; Hastbacka, et al., 1996; Makela, et al., 2002; Rossi and Superti-Furga, 2001). Moreover, disease-causing mutations identified SLC26A2, -A3 and -A4, are mutations within the STAS domains (Everett, et al., 1997; Hastbacka, et al., 1996; Makela, et al., 2002; Rossi and Superti-Furga, 2001). While these Slc26 proteins transport a variety of anions, play a variety of physiological roles, and are associated with several genetic disorders, the molecular components accounting for this diversity are only just being elucidated.

Slc26a9 functions as a Cl^--HCO_3^- exchanger, a Cl^- channel and a Na+ coupled transporter (Chang, et al., 2009b; Dorwart, et al., 2007; Xu, et al., 2005). The Slc26a9 protein is localized to epithelia of the stomach (Xu, et al., 2005) and lung (Chang, et al., 2009b; Lohi, et al., 2002; Xu, et al., 2005; Xu, et al., 2008), although mRNA is also detectable in brain, heart, kidney, small intestine, thymus, and ovary (Chang, et al., 2009b). Slc26a9 and CFTR have overlapping expression in gut and lung epithelia, making protein-protein interactions important. Slc26a9 channel and transporter activity is inhibited by interaction of its STAS domain with the R-region of CFTR in *Xenopus* oocytes (Chang, et al., 2009a). Interestingly, after cAMP-activation CFTR activity is enhanced with co-expression of SLC26A9 (NCBI accession number: NP_443166.1; MIM# 608481) in mammalian cells (Avella, et al., 2011b; Bertrand, et al., 2009). One group found that cellular HCO_3^- secretion leading to gastric surface pH increase is mediated by Slc26a9 Cl^--HCO_3^- exchange (Demitrack, et al., 2010). Slc26a9 deletion in mice causes decreased gastric acid secretion, loss of tubulovesicles (young mice) and reduction in parietal cells (adult mice) (Xu, et al., 2008). Human *SLC26A9* has become a novel candidate gene apparently associated with inner ear development (Urness, et al., 2010) as well as in antipsychotic responses (McClay, et al., 2011). Moreover, a recent GWAS analysis of Cystic Fibrosis patients indicates that expression of human SLC26A9 is associated with some CF phenotypes (Li, et al., 2011). Combined these studies have led to the hypothesis that *SLC26A9* mutations may impart large (monogenic) or small (polygenic) phenotypic effects in cystic fibrosis, stomach-related diseases and/or other diseases in humans. Thus, functional analyses of *SLC26A9* genetic polymorphisms are clinically important.

Recently, eight non-synonymous coding SNPs of *SLC26A9* were reported in the public SNP database (Table 1; http://www.ncbi.nlm.nih.gov/SNP/snp_ref.cgi?locusId=115019): Y70N

(rs75021701); T127N (rs77497889); I384T (rs112659452); R575W[1] (rs139697920); P606L (rs74146719); V622L (rs34992672); V744M (rs3811428) and H748R (rs16856462). This database reporting of human genetic variations, however, has not been complemented by functional or cell biological characterization. In this study, we examined the functional properties and the surface protein expression of SLC26A9 SNPs using the *Xenopus* oocyte expression system. Our results reveal critical roles of residues at positions 70 and 127 in determining the currents mediated by SLC26A9. Additionally our results indicate that the STAS domain is more than a structural motif and protein-interaction domain; STAS seems to also control SLC26A9 surface protein expression.

Methods and Materials

Animal health and welfare

X. laevis were housed and cared for in accordance and approval of the Institutional Care and Use Committees of Mayo Clinic College of Medicine.

SLC26A9 and its eight SNPs constructs

Subcloing triple FLAG-tagged SLC26A9—Cloning of *SLC26A9* (NM_052934.3) *and Slc26a9* (NM_177243.4) was recently reported by our group (Chang, et al., 2009b). The human *SLC26A9*'s opening reading frame was amplified by PCR reaction, sequence verified and subcloned into the *Xenopus* expression vector pGEMHE. The *SLC26A9*-pGEMHE was used as template for generating triple FLAG-tagged SLC26A9 (3FLAG-SLC26A9) by blunt ligation PCR. Two primers were used (forward primer: 5′ CATGATATCGACTACAAGGATGACGATGACAAGCAGCCCAGGCCCCGCT 3′ and reverse primer: 5′ ATCTTTATAATCACCGTCATGGTCTTTGTAGTCGCTCATATCTGGGGCATTTACA AGCA 3′, nucleotides coding for the tags are underlined) to insert a 66-bp sequence encoding a triple FLAG tag ("DYKDHDGDYKDHDIDYKDDDDK") after the first two residues ("MS-") of human SLC26A9. 3xFLAG did not alter function or expression of SLC26A9 or cSNPs.

Site-directed mutagenesis of human SLC26A9—Eight non-synonymous variants (Y70N, T127N, I384T, R575W, P606L, V622L, V744M and H748R; found in Table 1) were constructed by site-directed mutagenesis using the QuikChange site-directed mutagenesis kit (Stratagene, La Jolla, CA). For surface expression assay, the pGEMHE construct containing coding region for triple FLAG-tagged SLC26A9 was used as template for generating eight non-synonymous variants (Y70N, T127N, I384T, R575W, P606L, V622L, V744M and H748R). The positive clones were verified by sequencing prior to experiments. *SLC26A9* cSNPs (including constructs encoding the triple FLAG-tagged fusion proteins) were subcloned into pGEMHE (Chang, et al., 2009a; Chang, et al., 2009b). In the following section, the SLC26A9 indicate the "SLC26A9 - wild type" for functional analysis and "triple FLAG-tagged SLC26A9 - wild type" for surface protein expression detection. The SLC26A9-cSNPs (Y70N, T127N, I384T, R575W, P606L, V622L, V744M and H748R) indicate "triple FLAG-tagged cSNPs" for the surface protein expression detection.

Position predictions for SLC26A9-cSNPs

To predict SLC26A9 cSNP locations, an alignment of sequences of the cyanobacterial bicarbonate transporter – BicA (a member of SulP/SLC26 family), SHST1 (*Stylosanthes*

[1]R575W is replaced by R575Q in SLC26A9 cSNPs database (02/21/2012).

hamata high-affinity sulfate transporter), human SLC26A2 and human SLC26A9 was performed by ClustalW2 (Supp. Figure S1) (Larkin, et al., 2007). The border of SLC26A9 transmembrane regions are predicted by the topology of BicA (Shelden, et al., 2010). The border of STAS domain and its variable loop are based on the SpoIIAA and other Slc26 proteins (Aravind and Koonin, 2000; Pasqualetto, et al., 2010).

Oocyte experiments

Female *X. laevis* were purchased from Nasco (Fort Atkinson, WI). Oocytes were removed and collagenase dissociated (Romero, et al., 1998a; Romero, et al., 1998b). Capped cRNA was synthesized with the T7 mMessage mMachine kit (Ambion, Austin, TX). 50 nl of water or RNA solution (3ng cRNA coding for human SLC26A9 or cSNPs) were injected into stage V/VI *Xenopus* oocytes (Chang, et al., 2009a; Chang, et al., 2009b). Equal injected cRNA was confirmed by UV absorbance (A_{260}) and ethidium bromide staining (Supp. Figure S2). Oocytes were maintained at 16°C (OR3 media) and studied 3–7 days after injection.

Electrophysiology

Solutions—All solutions were either ND96 (96 mM NaCl, 2 mM KCl, 1.8 mM $CaCl_2$, 1 mM $MgCl_2$, 5 mM HEPES, pH 7.5) or iso-osmotic ion replacements (Table 2) (Chang, et al., 2009a; Chang, et al., 2009b; Sciortino and Romero, 1999).

Anion substitution—Bathing solutions were gravity perfused from the 140 ml syringes at ~5ml/min. With a chamber volume of 0.5ml, i.e., the bathing solution is completely changed in 15s. For anion substitution experiments, the bath solution was changed in the following order: 0 Cl^-/gluconate, Br^-, I^-, NO_3^-, SCN^-. The oocyte was maintained three minutes in each Cl^- replacement solution to make sure the current response was complete.

Two-Electrode Voltage Clamp—Electrodes were filled with 3 M KCl and had resistances of 0.2–0.5 megaohms. Oocytes were clamped at −60 mV, and current was constantly monitored and recorded at 10 Hz (Warner Inst. Co., Oocyte Clamp OC-725C). Voltage steps pulses (75 ms) were executed from −160 to +60 mV in 20 mV steps; the resulting I–V traces were filtered at 2 kHz (8 pole Bessel filter) and sampled at 10 kHz. Data were acquired and analyzed using Pulse and PulseFit (HEKA Instruments, Germany) (Chang, et al., 2009a; Chang, et al., 2009b; Sciortino and Romero, 1999). A KCl salt bridge was used to prevent artificial liquid junction when Cl^- was replaced by various anions.

Ion-Selective Microelectrodes—Ion-selective microelectrodes were manufactured and used to monitor pH_i and intracellular Cl^- ($[Cl^-]_i$) of oocytes as described previously (Chang, et al., 2009a; Chang, et al., 2009b; Romero, et al., 1998a; Romero, et al., 2000; Sciortino and Romero, 1999). Electrodes were connected to a high-impedance electrometer (WPI-FD223 for intracellular pH (pH_i) and V_m experiments), and digitized output data (filtered at 10Hz) were acquired at 0.5 Hz as previously (Chang, et al., 2009a; Chang, et al., 2009b; Romero, et al., 1998a; Romero, et al., 2000; Sciortino and Romero, 1999). All ion-selective microelectrodes had slopes of −54 to −57 mV/decade ion concentration (or activity). pH electrodes were calibrated at pH 6.0 and 8.0; and Cl^- electrodes were calibrated at 10mM NaCl and 100mM NaCl.

Calculations—Oocytes were perfused with ND96 for 5 min, at which time initial pH_i or initial pCl_i was measured. The solution was switched to CO_2/HCO_3^- for 8–10 min, and the final pH_i was measured at the stable trough. ΔpH_{CO2} = Final $pH_{i(CO2)}$ − Initial $pH_{i(CO2)}$; $\Delta pH_{(0Cl\text{-}CO2)}$ = Final $pH_{i(0Cl\text{-}CO2)}$ − Initial $pH_{i(0Cl\text{-}CO2)}$; $(dpH_i/dt)_{CO2}$ is the linear pH_i slope for a 15–45s segment at the pH_i trough. Likewise, $(dpH_i/dt)_{(0Cl\text{-}CO2)}$ is the linear pH_i slope

during the response to $0Cl^-$. $[HCO_3^-]_i$ was calculated from the Henderson-Hasselbach equation (Roos and Boron, 1981). $\Delta[Cl^-]_i$ = Final pCl_i – Initial pCl_i; $\Delta d[Cl^-]_i/dt = \Delta[Cl^-]_i/t$ (min); "n" indicates the total number of experiments, and oocytes were harvested from at least two donor animals.

Oocyte Surface Protein Expression

Oocyte surface protein expression of human SLC26A9 and its eight SNPs were measured using biotinylation as well as immunolocalization.

Biotinylation assay—Cell surface protein isolation kit (Pierce, Rockford, IL) was used according to the manufacturer instructions. 72 h after cRNA injection (3ng), groups of 20 oocytes were incubated for 1h at 4°C in PBS that contained 0.25mg/ml Sulfo-NHS-biotin. Then, the non-reactive biotin was quenched and cells were disrupted by lysis buffer with protease inhibitor cocktail (Sigma P8340). The homogenate was incubated at 4°C with rotation mixing for 1 h, and then incubated with neutravidin agarose in the mini-column (kit). The non-bound proteins were washed from the column. The bound, biotinlyated protein was eluted from the column by SDS sample buffer containing 50mM DTT, precipitated and size-fractionated by SDS-PAGE, then transferred onto PVDF membrane. The PVDF membrane was blocked in 5% non-fat milk/PBST and then probed with an anti-FLAG mouse monoclonal primary antibody overnight at 4°C. After washing and incubation with secondary antibodies - HRP-conjugated goat-anti-mouse polyclonal antibody, the immunoblotted proteins were visualized using SuperSignal West Pico Chemiluminescent Substrate (Thermo Scientific). Experiments were repeated at least 3 times and results from representative immunoblots are shown.

Immunolocalization—*Xenopus* oocytes were injected with H_2O or 3ng cRNAs coding for triple-FLAG tagged human SLC26A9 or its eight non-synonymous SNPs (3xFLAG-SNP) respectively. Three days after injection, the oocytes were fixed in 4% PFA/PBS for 1 h, followed by 100 mM glycine in PBS for 30 min. Then the oocytes were stored in 30% sucrose at 4°C overnight and frozen in OCT compound (Tissue-tek) with liquid nitrogen. 10 μm cryostat sections were cut, the sections were blocked in 5% non-fat milk, 1% BSA in PBS for 1h. Oocytes stained with only the secondary antibody were controls for background staining. Mouse monoclonal anti-FLAG primary antibody was used at a dilution of 1:1000 overnight, followed by incubation with a secondary anti-mouse Cy3 antibody at a dilution of 1:1,000. Sections were observed using fluorescent microscopy (Zeiss Observer Z1), and images were collected using the AxioVision program (Zeiss).

Statistical analysis

Ion activities or currents are quantified as the mean ± s.e.m (6–12 oocytes in each experimental group from at least two donor *Xenopus*). Statistical analysis was performed with One-way ANOVA and pairwise comparison between groups was performed using Tukey test ($p < 0.05$; MINITAB software, USA).

Results

Coding non-synonymous single nucleotide polymorphisms (SNPs) of SLC26A9

In the NCBI SNP database, eight coding, non-synonymous nucleotide polymorphisms of human *SLC26A9* are publically available (Table 1). The mutations resulting from these missense SNPs of SLC26A9 are Y70N (rs75021701); T127N (rs77497889); I384T (rs112659452); R575W (rs139697920); P606L (rs74146719); V622L (rs34992672); V744M (rs3811428) and H748R (rs16856462). To postulate possible roles of these cSNP mutants, we made a topology prediction for SLC26A9 (Figure 1A). The SLC26A9 transmembrane

topology is based on the cyanobacterial bicarbonate transporter (BicA), a member of SulP (SLC26) family (Shelden, et al., 2010). The border of STAS domain and its variable loop are based on the alignment with SpoIIAA protein and other Slc26 proteins (Aravind and Koonin, 2000; Pasqualetto, et al., 2010). Figure 1A illustrates the predicted locations of these cSNPs: Y70N (rs75021701in cytoplasmic N-terminus and close to the TM-1 (transmembrane domain 1); T127N (rs77497889) in TM-3; I384T (rs112659452) in an intracellular loop between TM-8 and -9; R575W (rs139697920), P606L (rs74146719) and V622L (rs34992672) in the variable loop of STAS domain; V744M (rs3811428) and H748R (rs16856462) in the C-terminus close to the STAS domain.

We postulated that conserved residues should play important roles in ion transport function or trafficking of the SLC26A9 proteins to the cell surface. Next, to determine the potential significance of these residues, we made an alignment for Slc26a9 proteins from ifferent species (Figure 1B). Among these eight mutated residues; Y70, T127, I384 and R575 are conserved in Slc26a9 proteins of mammalian species including chimpanzee, horse, mouse and rat. Notably, T127 belongs to a high conservative sequence (-VPGTFAV-) of Slc26a9 proteins. And the “GxF” motif is conserved among all Slc26 members except SLC26A11 (data not shown).

Several cSNPs change SLC26A9 Cl^- current magnitude

Large Cl^- currents have been reported from two-electrode voltage clamp in the *Xenopus* oocytes expressing mouse Slc26a9 (Romero, et al., 2006) or human SLC26A9 (Dorwart, et al., 2007). To understand the possible SLC26A9 cSNPs pathophysiology, these point mutations were created in the template of SLC26A9 and expressed in *Xenopus* oocytes for functional analysis. The Cl^- current (Figure 2A) of control oocytes injected with *SLC26A9's* cRNA was compared with that of oocytes injected with same amount cRNA (Supp. Figure S2) of the eight SLC26A9 cSNPs. The oocytes were clamped at −60 mV. As previously reported for mouse Slc26a9 (Chang, et al., 2009b) and human SLC26A9 (Dorwart, et al., 2007), SLC26A9 ($I_{SLC26A9}$; Figure 2A; Figure 3A, B- black) showed large voltage-dependent I (I–V)-responses which were reduced, changed reversal potential (E_{rev}) and slightly rectified when bath Cl^- was replaced by gluconate (0 Cl^-/ND96 solution, pH7.5). Compared with $I_{SLC26A9}$, four cSNPs changed current magnitudes with statistical significance ($p<0.01$) (Figure 2A) but had similar overall I–V shapes (Figure 3A, B). Y70N (rs75021701) (Figure 3A, B-blue) responded to similar maneuvers with larger than wild-type currents. Conversely, smaller $I_{SLC26A9}$'s were elicited in T127N (rs77497889), V622L (rs34992672) and V744M (rs3811428) in the presence or absence of Cl^- (Figure 2A; Figure 3A, B- red). The I–V relationships illustrate that these changes are maintained over the entire voltage range tested (Figure 3B). To highlight the differences among the SLC26A9 and its cSNPs, currents are plotted at +60mV in the ND96 solution (Figure 3A). Figure 3A shows that I_{Y70N} is ~two fold increased (15.81±2.2 μA, $p<0.01$) at +60 mV compared to $I_{SLC26A9}$ (8.08 ± 1.47 μA). T127N (rs77497889), V622L (rs34992672) and V744M (rs3811428) both display decreased currents at +60 mV (ND96) ($n\geq6$, $p<0.005$) (Figure 3A). None of these SLC26A9/cSNPs-currents were observed in the water-control oocytes (data not shown), as previous report (Chang, et al., 2009b).

Cell surface detection of SLC26A9 and its non-synonymous cSNPs

To investigate the effect of SLC26A9 cSNPs on protein expression and trafficking, cell surface biontinylation assay and immunohistochemistry assays were performed on *Xenopus* oocytes expressing SLC26A9 and its cSNPs. To maximize the specificity of detection, we subcloned a triple FLAG epitope fused to the N-terminus of human SLC26A9 and its eight cSNPs respectively (see Materials and Methods). This 3xFLAG-tag allowed us to use a mouse anti-FLAG monoclonal for protein detection of all of the constructs. Voltage clamp

experiments found that these triple FLAG tagged SLC26A9/cSNPs show the same function as its non-tagged counterparts respectively (data not shown), especially for Y70N (rs75021701), T127N (rs77497889) and V622L (rs34992672). Thus the constructs encoding the triple FLAG tagged SLC26A9/cSNPs were used in our surface expression detection experiments (Figure 2B,C).

As shown in Figure 2B, the cell surface expression was detected by biotinylation assay for SLC26A9 and its eight cSNPS. The band corresponding to SLC26A9/cSNPs is 100kD, which is close to the predicted monomer size of triple FLAG-tagged SLC26A9 protein (813 amino acid, 90kD). No bands were detected for the control water-injected oocytes suggesting the signals were responsible for SLC26A9/cSNPs surface expression. Although it was not quantified, the bands corresponding to Y70N (rs75021701), P606L (rs74146719), V622L (rs34992672), V744M (rs3811428) and H748R (rs16856462) were slightly less in density than the band for SLC26A9 while the bands for T127N (rs77497889), I384T (rs112659452) and R575W (rs139697920) were similar or slightly higher in density than the band for SLC26A9 in three independent experiments.

To further detect the surface protein expression level of Y70N (rs75021701), T127N (rs77497889) and V622L (rs34992672), immunohistochemistry of crysectioned oocytes was used, followed by protein detection with the anti-FLAG antibody (Figure 2C). The fluorescence signals on plasma membrane of oocytes expressing T127N (rs77497889) are similar to that of SLC26A9, while the fluorescence signals for Y70N (rs75021701) and V622L (rs34992672) are slightly less than that of SLC26A9. These results are consistent with those of the biotinylation experiments.

Y70N activates Cl^--HCO_3^- exchange by SLC26A9

Several groups' studies suggest that SLC26A9 (and mouse Slc26a9) function not only as a Cl^- channel (Bertrand, et al., 2009; Chang, et al., 2009b; Dorwart, et al., 2007; Xu, et al., 2005; Xu, et al., 2008) but also a Cl^--HCO_3^- exchanger (Bertrand, et al., 2009; Chang, et al., 2009b; Dorwart, et al., 2007; Xu, et al., 2005; Xu, et al., 2008). Since large Cl^- currents (Cl^- channel activity) were observed for Y70N (rs75021701) (Figure 2A; Figure 3A), we sought to determine if the Cl^--HCO_3^- exchanger activity was simultaneously enhanced. To more directly evaluate Cl^--HCO_3^- exchange activity, we used pH microelectrodes to measure intracellular pH (pH_i) changes after Cl^- removal and readdition from a CO_2/HCO_3^- bath solution for SLC26A9 and Y70N (Figure 4A, B). In water controls, Cl^- replacement (with gluconate; $0Cl^-$) did not change pH_i or V_m (data not shown), as previously described (Chang, et al., 2009b). However, Figure 4B illustrates that Y70N increased Cl^--HCO_3^- exchange activity, i.e., Y70N had an obvious depolarization and increased pH_i change (initial rate = $+57\times10^{-5}$ pH unit/sec) after switching to the 0 Cl^-/5%CO_2 buffer. SLC26A9 (Figure 4A) alkalized at $+31\times10^{-5}$ pH unit/sec. These results illustrate that Y70N exhibits increased SLC26A9 function, both as a Cl^- channel and as a Cl^--HCO_3^- exchanger (Table 3).

T127N decreases conductance of Cl^-, Br^-, I^-, but neither NO_3^- nor SCN^-

Based on the very low currents of T127N (rs77497889), we reasoned that the Cl^-/HCO_3^- exchange of T127N (rs77497889) is only slightly different from the water–injected control oocytes. T127N (rs77497889) is the only SLC26A9 cSNP located in the transmembrane domain (Figure 1A), and transmembrane domains often play important roles in solute permeation of channels, and thus control ionic conductance. We focused on the anion conductance of T127N, rather than Cl^-/HCO_3^- exchange. To further characterize the T127N-mediated current, we measured its conductance of different monovalent anions (Cl^-, Br^-, I^-, NO_3^- and SCN^-) compared to those of SLC26A9. We found an anion selectivity of

SLC26A9 was similar to that previously reported (Dorwart, et al., 2007). That is, SLC26A9 conducted Br^- similar to Cl^-, but better than I^- and NO_3^- (Figure 5A, C). We also found SLC26A9 conducted isothiocyanate (SCN^-), and that the conductance of SCN^- greater than that of I^- and NO_3^- but slightly less than that of Br^- and Cl^-. Thus, SLC26A9 anion conductance has the rank order: $Cl^- \approx Br^- > SCN^- > I^- > NO_3^- \gg Glu^-$. Figure 5B, C illustrates that I_{T127N} had decreased conductance of not only for Cl^- but also of Brand I^- compared to $I_{SLC26A9}$. However, the current carried by NO_3^- and SCN^- were not decreased by T127N (rs77497889) compared to that of SLC26A9. Thus, the anion conductance of I_{T127N} differed from SLC26A9: $SCN^- > Cl^- \approx Br^- > I^- > NO_3^- \gg Glu^-$. With similar ionic replacements (Cl^-, Br^-, I^-, NO_3^- and SCN^-), water-injected oocytes display only minor currents (<100nA) (data not shown).

V622L reduces SLC26A9 function

Recently, STAS domains have emerged as a major form of regulation for SLC26 family transporters/channels (Chang, et al., 2009a; Ko, et al., 2004; Shcheynikov, et al., 2006a). V622L (rs34992672) is one of the cSNPs located in the STAS domain (Figure 1A) which changed SLC26A9 function. Although the surface protein expression of V622L is slightly reduced (Figure 2B,C), function may also be impaired. Again, we used pH_i to quantify Cl^--HCO_3^- exchanger activity of V622L. As shown in Figure 4C shows that V622L reduced Cl^--HCO_3^- exchanger activity, i.e., V622L has a smaller depolarization and pH_i change (initial rate (dpH_i/dt) = $+23\times10^{-5}$ pH unit/sec after Cl^- removal in the CO_2/HCO_3^- buffer; Table 3). These results indicate that V622L decreased SLC26A9 Cl^--HCO_3^- exchange function, yet they are complicated due to simultaneous decrease protein expression.

Discussion

SLC26A9 protein functions as both a chloride channel and a Cl^--HCO_3^- exchanger involved in Cl^- and HCO_3^- absorption as well as secretion in various epithelia (Chang, et al., 2009b; Dorwart, et al., 2007; Lohi, et al., 2002; Loriol, et al., 2008; Xu, et al., 2005). Numerous mutations in *SLC26* genes have been shown to lead to human disorders (Dawson and Markovich, 2005; Everett and Green, 1999; Liu, et al., 2003; Markovich, 2001; Sindic, et al., 2007) and these disorders underscore the need to further our understanding of the *SLC26* genes in human disease. Recently, a genome-wide association studies (GWAS) of neurocognition, as an indicator of antipsychotic treatment response in Schizophrenia, identified that one intronic SNP (rs11240594) of *SLC26A9* was associated with olanzapine effects on neuro-processing speed, $p = 1.4\times10^{-7}$) (McClay, et al., 2011). These investigators also noted that multiple neighboring SNPs were in linkage disequilibrium with this *SLC26A9* SNP (rs11240594), apparently tagging the same signal (McClay, et al., 2011). These linkage data indicate that *SLC26A9* gene is tightly linked with multiple neurocognitive domains in the brain and the patients with *SLC26A9* allelic variations (i.e., cSNPs) may have increased risk of schizophrenia or brain dysfunction.

Deletion of *Slc26a9* in mice resulted in the loss of gastric acid secretion and a moderate reduction in the number of parietal cells (Xu, et al., 2008). Microarray analysis and *in situ* hybridization showns that *Slc26a9* is down-regulated in *Fgf3*$^{-/-}$; *Fgf10*$^{-/-}$ (Fibroblast growth factor) *mouse* embryos (Urness, et al., 2010). Together these data and the human association of McClay and coworkers suggest that SLC26A9/Slc26a9 play multiple physiological roles being associated with human antipsychotic response, gastric acid secretion and otic development. These varied findings prompted us to investigate the potential effect of eight missense cSNPs of SLC26A9.

Y70N: a cSNP in cytoplasmic N-terminus

Little is known about the regulation and the structural elements of the N-terminus of Slc26 proteins as there are no crystal structures of Slc26 protein TMs or N-termini. There is expanding data that the N-termini of certain anion channels control function. For example, CFTR studies suggest that the cytoplasmic N-terminus is critical for the biosynthesis of this cAMP-activated chloride channel (Prince, et al., 1999). The CFTR N-terminus also controls PKA-dependent channel gating by interaction of the R-region via its highly conserved acidic stretch (Chappe, et al., 2005; Naren, et al., 1999). Moreover, the CFTR N-terminus physically links CFTR to proteins involved into membrane trafficking machinery (Bilan, et al., 2004; Naren, et al., 1998; Peters, et al., 2001). Several AP (adaptor protein complex) and GGA (Golgi-localized, γ-ear containing, Arf-binding adaptor protein) binding sites have been identified in the cytoplasmic, ClC chloride channel's N-termini (Stauber and Jentsch, 2010). With these findings, we hypothesize that the SLC26A9 N-terminus may also play important functional roles. Our experiments reveal that Y70N displays enhanced SLC26A9 function. Y70 is located in between the SLC26A9 N-terminus and the first TM. These data, with our topology model, suggest that Y70 may be in a region of inter-domain structural flexibility which in turn amplifies activity.

T127N: a cSNP in the transmembrane domain

Multiple structure-function studies with CFTR have defined the molecular-level importance of critical functional domains and have correlated CFTR mutations with their clinical outcome (Hanrahan and Wioland, 2004; Sheppard and Welsh, 1999). However, the structure-function studies for the SLC26 family are just beginning. Recently Ohana *et al.* found by modeling the Slc26a6 TM onto the ClC chloride channel's structure, two conserved negative residues E357 (Slc26a6) and E367 (Slc26a3) which play key roles in their unique transport modes (Ohana, et al., 2011). On the other hand, a significant number of conserved polar residues in transmembrane helices 1 and 2 of SulP family (plant and bacteria Slc26 family) were found by sequence and bioinformatics analysis (Leves, et al., 2008). Functional analysis results from SHST1-mutations (sulfate transporter) suggest that removal of even a single OH- group from these polar residues significantly affects transport. Figure 1A illustrates that T127N is predicted in TM-3 of SLC26A9, and I_{T127N} anion conductance is decreased for Cl^-, Br^- and I^-, yet unchanged for NO_3^- and SCN^- (Figure 3, Figure 5). Interestingly, $I_{T127N}(SCN^-)$ is the same magnitude as $I_{SLC26A9}(SCN^-)$ and is dramatically increased from the basal current for T127N. Our sequence analysis revealed that the polar residue T127 is embedded in an undefined motif (GXF) which is highly conserved from SLC26A1 to SLC26A9 (not shown). We hypothesize that the polar T127 residue is located in a critical position adjacent to the SLC26A9 channel pore. By extension, T127N would then subtly change the pore conformation for some compact anions (Cl^-, $Br^-$and I^-) but not for a resonant anion (NO_3^- and SCN^-). Clearly, additional investigations will be needed to define the structural role of T127 in SLC26A9 function.

V622L: a cSNP in the STAS domain variable loop

Functional interactions of Slc26a3 and Slc26a6 STAS domains (C-terminus) with the R-region of CFTR have been previously reported to cause mutual stimulation of Slc26-activity and CFTR-channel activity (Ko, et al., 2004; Rakonczay, et al., 2008; Shcheynikov, et al., 2004).The situation appears more complex for the relationship of Slc26a9/SLC26A9 and R-CFTR We recently demonstrated that Slc26a9 function (Cl^- channel and Cl^--HCO_3^- exchange) is inhibited by interaction of the CFTR R-region and the Slc26a9-STAS domain (Chang, et al., 2009a). This (R-region)-STAS interaction in *Xenopus* oocytes or of proteins in solution, did not require activation of PKA (Chang, et al., 2009a). Using HBE (human bronchial epithelial) cells, Bertrand *et al.* found SLC26A9 functions as an anion conductance which requires a functional interaction with PKA-activated CFTR (Bertrand, et

al., 2009). Another group found SLC26A9 favors the biogenesis and/or stabilization of CFTR, leading to stimulated currents even with a non-SNP-mutation (L638P) which kills SLC26A9 function (Avella, et al., 2011a

Our knowledge of the STAS domain of Slc26 proteins stems from STAS' weak but significant similarity with the Bacillus antisigma protein SpoIIAA (Aravind and Koonin, 2000). By mapping the conserved motifs onto Prestin STAS structure (Babu, et al., 2010; Pasqualetto, et al., 2010), the STAS domain seems to consist of six β-strands, surrounded by five α-helices. Babu and coworkers solved the STAS structure of *E.coli* YchM, finding the same basic structure, but that YchM is tightly associated with an acyl carrier protein and tightly associated with fatty acid synthesis (Babu, et al., 2010).The significance of this finding for vertebrate Slc26 proteins and their STAS-domains is currently unknown.

Our analysis using a multiple sequence alignment indicates that there is sequence of variable length (variable loop) between the first α helix and the third β strand of Slc26 STAS domains. This variable loop also separates the STAS domain into two sequence-conserved regions. Interestingly the structure solved for prestin deleted this variable loop (Pasqualetto, et al., 2010); and YchM does not contain such an intervening sequence (Babu, et al., 2010). Without structure information for this STAS variable loop, we cannot anticipate or predict STAS structural elements or their potential regulatory roles. V622L is located in the SLC26A9 STAS domain within the variable loop (residues 562-654). In *M. musculus*, *R. norvegicus* and *X. tropicalis*, V622 is replaced by I622, a similar hydrophobic amino acid. V622L reduces the SLC26A9 Cl^- current and Cl^--HCO_3^- exchange activity, but also slightly reduces protein expression. Despite only minor protein reduction, function of V622L-SLC26A9 is ~50% of wild-type SLC26A9. Thus, this cSNP in the STAS domain has an effect on both protein expression and activity of the resultant transporter-channel. Other experiments indicate that V622I increases $I_{SLC26A9}$ (Chen and Romero, 2010). We postulate that replacement of I622 by V622 or L622 might cause progressive yet subtle alterations in conformation which result in changes of STAS domain tertiary structure. This change would then interfere with required interactions with other proteins or interdomain-regions. Together these findings indicate that the V622 is a controller of transport activity magnitude and proteins expression, and that side chain length of 622 has a role in controlling activity level.

Summary

We have functionally assessed eight missense cSNPs of SLC26A9. Four SLC26A9 cSNPs show significantly altered transport functions from wild-type: Y70N increased Cl^- currents, while T127N, V622L and V744M decreased Cl^- currents. Additionally, Y70N increased Cl^--HCO_3^- exchange activity, but T127N and V622L displayed decreased Cl^--HCO_3^- exchanger activity. The effects of T127N are more subtle: (a) $I_{SLC26A9}$ was decreased for Cl^-, Br^- and I^-, (b) $I_{SLC26A9}$ was unchanged for NO_3^- and SCN^-. That is, the anion conductance order of SLC26A9 was changed by T127N. Thus, we predicted that allelic variations in human SLC26A9 should change epithelial Cl^- transport: N70 polymorphism would increase Cl^- transport across epithelial cells while the others with N127, L622, and M744 polymorphisms would reduce Cl^- transport. Thus, any disorder resulting from SLC26A9 interaction or functional presence (e.g., cystic fibrosis), would also be predicted to have altered pathophysiology due to allelic variations of SLC26A9.

Supplementary Material

Refer to Web version on PubMed Central for supplementary material.

Acknowledgments

We thank Heather L. Holmes and Elyse M. Scileppi for technical assistance.

We gratefully acknowledge the Support of NIH (R01-EY017732, P30-DK090728) and the Mayo Clinic Foundation.

References

Aravind L, Koonin EV. The STAS domain - a link between anion transporters and antisigma-factor antagonists. Curr Biol. 2000; 10(2):R53–5. [PubMed: 10662676]

Avella M, Borgese F, Ehrenfeld J. Characterization of the L683P mutation of SLC26A9 in Xenopus oocytes. Biochim Biophys Acta. 2011a; 1810(6):577–83. [PubMed: 21439353]

Avella M, Loriol C, Boulukos K, Borgese F, Ehrenfeld J. SLC26A9 stimulates CFTR expression and function in human bronchial cell lines. J Cell Physiol. 2011b; 226(1):212–23. [PubMed: 20658517]

Babu M, Greenblatt JF, Emili A, Strynadka NC, Reithmeier RA, Moraes TF. Structure of a SLC26 anion transporter STAS domain in complex with acyl carrier protein: implications for E. coli YchM in fatty acid metabolism. Structure. 2010; 18(11):1450–62. [PubMed: 21070944]

Bertrand CA, Zhang R, Pilewski JM, Frizzell RA. SLC26A9 is a constitutively active, CFTR-regulated anion conductance in human bronchial epithelia. J Gen Physiol. 2009; 133(4):421–38. [PubMed: 19289574]

Bilan F, Thoreau V, Nacfer M, Derand R, Norez C, Cantereau A, Garcia M, Becq F, Kitzis A. Syntaxin 8 impairs trafficking of cystic fibrosis transmembrane conductance regulator (CFTR) and inhibits its channel activity. J Cell Sci. 2004; 117(Pt 10):1923–35. [PubMed: 15039462]

Bissig M, Hagenbuch B, Stieger B, Koller T, Meier PJ. Functional expression cloning of the canalicular sulfate transport system of rat hepatocytes. J Biol Chem. 1994; 269(4):3017–21. [PubMed: 8300633]

Chang M-H, Plata C, Sinđić A, Ranatunga WK, Chen AP, Zandi-Nejad K, Chan KW, Thompson J, Mount DB, Romero MF. Slc26a9 is inhibited by the R-region of CFTR via the STAS domain. J Biol Chem. 2009a; 284(28306-18):28306–18. [PubMed: 19643730]

Chang M-H, Plata C, Zandi-Nejad K, Sindic A, Sussman CR, Mercado A, Broumand V, Raghuram V, Mount DB, Romero MF. Slc26A9 - anion exchanger, channel and Na^+ transporter. J Membr Biol. 2009b; 128(3):125–40.

Chappe V, Irvine T, Liao J, Evagelidis A, Hanrahan JW. Phosphorylation of CFTR by PKA promotes binding of the regulatory domain. Embo J. 2005; 24(15):2730–40. [PubMed: 16001079]

Chen A-P, Romero MF. Channel inhibitory region within the STAS domain of human SLC26A9. Faseb J. 2010; 24:1002.7.

Cherest H, Davidian JC, Thomas D, Benes V, Ansorge W, Surdin-Kerjan Y. Molecular characterization of two high affinity sulfate transporters in Saccharomyces cerevisiae. Genetics. 1997; 145(3):627–35. [PubMed: 9055073]

Dawson PA, Markovich D. Pathogenetics of the human SLC26 transporters. Curr Med Chem. 2005; 12(4):385–96. [PubMed: 15720248]

Demitrack ES, Soleimani M, Montrose MH. Damage to the gastric epithelium activates cellular bicarbonate secretion via SLC26A9 Cl(−)/HCO(3)(−). Am J Physiol Gastrointest Liver Physiol. 2010; 299(1):G255–64. [PubMed: 20413716]

Detro-Dassen S, Schanzler M, Lauks H, Martin I, Berstenhorst SM, Nothmann D, Torres-Salazar D, Hidalgo P, Schmalzing G, Fahlke C. Conserved Dimeric Subunit Stoichiometry of SLC26 Multifunctional Anion Exchangers. J Biol Chem. 2008; 283(7):4177–88. [PubMed: 18073211]

Dorwart MR, Shcheynikov N, Wang Y, Stippec S, Muallem S. SLC26A9 is a Cl channel regulated by the WNK kinases. J Physiol. 2007; 584(Pt 1):333–45. [PubMed: 17673510]

Dorwart MR, Shcheynikov N, Yang D, Muallem S. The solute carrier 26 family of proteins in epithelial ion transport. Physiology (Bethesda). 2008; 23:104–14. [PubMed: 18400693]

Everett LA, Glaser B, Beck JC, Idol JR, Buchs A, Heyman M, Adawi F, Hazani E, Nassir E, Baxevanis AD, et al. Pendred syndrome is caused by mutations in a putative sulphate transporter gene (PDS). Nat Genet. 1997; 17(4):411–22. [PubMed: 9398842]

Everett LA, Green ED. A family of mammalian anion transporters and their involvement in human genetic diseases. Hum Mol Genet. 1999; 8(10):1883–91. [PubMed: 10469841]

Hanrahan JW, Wioland MA. Revisiting cystic fibrosis transmembrane conductance regulator structure and function. Proc Am Thorac Soc. 2004; 1(1):17–21. [PubMed: 16113406]

Hastbacka J, Superti-Furga A, Wilcox WR, Rimoin DL, Cohn DH, Lander ES. Atelosteogenesis type II is caused by mutations in the diastrophic dysplasia sulfate-transporter gene (DTDST): evidence for a phenotypic series involving three chondrodysplasias. Am J Hum Genet. 1996; 58(2):255–62. [PubMed: 8571951]

Hawkesford MJ. Transporter gene families in plants: the sulfate transporter gene family— redundancy or specialization? Physiol Plant. 2003; 117:155–163.

Homma K, Miller KK, Anderson CT, Sengupta S, Du GG, Aguinaga S, Cheatham M, Dallos P, Zheng J. Interaction between CFTR and prestin (SLC26A5). Biochim Biophys Acta. 2010; 1798(6): 1029–40. [PubMed: 20138822]

Jiang Z, Grichtchenko, Boron WF, Aronson PS. Specificity of anion exchange mediated by mouse Slc26a6. J Biol Chem. 2002; 277(37):33963–7. [PubMed: 12119287]

Karniski LP, Lotscher M, Fucentese M, Hilfiker H, Biber J, Murer H. Immunolocalization of sat-1 sulfate/oxalate/bicarbonate anion exchanger in the rat kidney. Am J Physiol. 1998; 275(1 Pt 2):F79–87. [PubMed: 9689008]

Kim KH, Shcheynikov N, Wang Y, Muallem S. SLC26A7 Is a Cl^- Channel Regulated by Intracellular pH. J Biol Chem. 2005; 280(8):6463–70. [PubMed: 15591059]

Ko SB, Shcheynikov N, Choi JY, Luo X, Ishibashi K, Thomas PJ, Kim JY, Kim KH, Lee MG, Naruse S, et al. A molecular mechanism for aberrant CFTR-dependent HCO_3^- transport in cystic fibrosis. Embo J. 2002; 21(21):5662–72. [PubMed: 12411484]

Ko SB, Zeng W, Dorwart MR, Luo X, Kim KH, Millen L, Goto H, Naruse S, Soyombo A, Thomas PJ, et al. Gating of CFTR by the STAS domain of SLC26 transporters. Nat Cell Biol. 2004; 6(4):343–50. [PubMed: 15048129]

Larkin MA, Blackshields G, Brown NP, Chenna R, McGettigan PA, McWilliam H, Valentin F, Wallace IM, Wilm A, Lopez R, et al. Clustal W and Clustal X version 2.0. Bioinformatics. 2007; 23(21):2947–8. [PubMed: 17846036]

Leves FP, Tierney ML, Howitt SM. Polar residues in a conserved motif spanning helices 1 and 2 are functionally important in the SulP transporter family. Int J Biochem Cell Biol. 2008; 40(11):2596–605. [PubMed: 18585087]

Li, X.; Corvol, H.; Li, W.; Chiang, T.; Lin, F.; Boelle, P-Y.; Drumm, M.; Cutting, G.; Knowles, M.; Durie, P., et al. Replication evidence that constituents of the apical plasma membrane contribute to Meconium ileus in Cystic Fibrosis. 25th N Am CF Conference; 2011.

Liu XZ, Ouyang XM, Xia XJ, Zheng J, Pandya A, Li F, Du LL, Welch KO, Petit C, Smith RJ, et al. Prestin, a cochlear motor protein, is defective in non-syndromic hearing loss. Hum Mol Genet. 2003; 12(10):1155–1162. [PubMed: 12719379]

Lohi H, Kujala M, Makela S, Lehtonen E, Kestila M, Saarialho-Kere U, Markovich D, Kere J. Functional characterization of three novel tissue-specific anion exchangers SLC26A7, -A8, and -A9. J Biol Chem. 2002; 277(16):14246–54. [PubMed: 11834742]

Loriol C, Dulong S, Avella M, Gabillat N, Boulukos K, Borgese F, Ehrenfeld J. Characterization of SLC26A9, facilitation of Cl^- transport by bicarbonate. Cell Physiol Biochem. 2008; 22(1–4):15–30. [PubMed: 18769029]

Makela S, Kere J, Holmberg C, Hoglund P. SLC26A3 mutations in congenital chloride diarrhea. Hum Mutat. 2002; 20(6):425–38. [PubMed: 12442266]

Markovich D. Physiological roles and regulation of mammalian sulfate transporters. Physiol Rev. 2001; 81(4):1499–533. [PubMed: 11581495]

McClay JL, Adkins DE, Aberg K, Bukszar J, Khachane AN, Keefe RS, Perkins DO, McEvoy JP, Stroup TS, Vann RE, et al. Genome-wide pharmacogenomic study of neurocognition as an

indicator of antipsychotic treatment response in schizophrenia. Neuropsychopharmacology. 2011; 36(3):616–26. [PubMed: 21107309]

Moseley RH, Hoglund P, Wu GD, Silberg DG, Haila S, de la Chapelle A, Holmberg C, Kere J. Downregulated in adenoma gene encodes a chloride transporter defective in congenital chloride diarrhea. Am J Physiol. 1999; 276(1 Pt 1):G185–92. [PubMed: 9886994]

Mount DB, Romero MF. The SLC26 gene family of multifunctional anion exchangers. Pflügers Arch. 2004; 447(5):710–21.

Naren AP, Cormet-Boyaka E, Fu J, Villain M, Blalock JE, Quick MW, Kirk KL. CFTR chloride channel regulation by an interdomain interaction. Science. 1999; 286(5439):544–8. [PubMed: 10521352]

Naren AP, Quick MW, Collawn JF, Nelson DJ, Kirk KL. Syntaxin 1A inhibits CFTR chloride channels by means of domain-specific protein-protein interactions. Proc Natl Acad Sci U S A. 1998; 95(18):10972–7. [PubMed: 9724814]

Ohana E, Shcheynikov N, Yang D, So I, Muallem S. Determinants of coupled transport and uncoupled current by the electrogenic SLC26 transporters. J Gen Physiol. 2011; 137(2):239–51. [PubMed: 21282402]

Pasqualetto E, Aiello R, Gesiot L, Bonetto G, Bellanda M, Battistutta R. Structure of the cytosolic portion of motor protein prestin and functional role of the STAS domain in SLC26/SulP anion transporters. J Mol Biol. 2010; 400:448–462. [PubMed: 20471983]

Peters KW, Qi J, Johnson JP, Watkins SC, Frizzell RA. Role of snare proteins in CFTR and ENaC trafficking. Pflugers Arch. 2001; 443(Suppl 1):S65–9. [PubMed: 11845306]

Prince LS, Peter K, Hatton SR, Zaliauskiene L, Cotlin LF, Clancy JP, Marchase RB, Collawn JF. Efficient endocytosis of the cystic fibrosis transmembrane conductance regulator requires a tyrosine-based signal. J Biol Chem. 1999; 274(6):3602–9. [PubMed: 9920908]

Rakonczay Z Jr, Hegyi P, Hasegawa M, Inoue M, You J, Iida A, Ignath I, Alton EW, Griesenbach U, Ovari G, et al. CFTR gene transfer to human cystic fibrosis pancreatic duct cells using a Sendai virus vector. J Cell Physiol. 2008; 214(2):442–55. [PubMed: 17654517]

Riordan JR, Rommens JM, Kerem B, Alon N, Rozmahel R, Grzelczak Z, Zielenski J, Lok S, Plavsic N, Chou JL, et al. Identification of the cystic fibrosis gene: cloning and characterization of complementary DNA. Science. 1989; 245(4922):1066–73. [PubMed: 2475911]

Rode B, Dirami T, Bakouh N, Rizk-Rabin M, Norez C, Lhuillier P, Lores P, Jollivet M, Melin P, Zvetkova I, et al. The testis anion transporter TAT1 (SLC26A8) physically and functionally interacts with the cystic fibrosis transmembrane conductance regulator channel: a potential role during sperm capacitation. Hum Mol Genet. 2012; 21(6):1287–98. [PubMed: 22121115]

Romero MF, Chang M-H, Plata C, Zandi-Nejad K, Broumand V, Sussman CR, Mount DB. "Physiology of electrogenic SLC26 paralogs" In - Epithelial Anion Transport in Health and Disease: the role of the SLC26 transporters family. Novartis Foundation Symposium. 2006; 273:126–147. [PubMed: 17120765]

Romero MF, Fong P, Berger UV, Hediger MA, Boron WF. Cloning and functional expression of rNBC, an electrogenic Na^+-HCO_3^- cotransporter from rat kidney. Am J Physiol. 1998a; 274(2 Pt 2):F425–32. [PubMed: 9486238]

Romero MF, Henry D, Nelson S, Harte PJ, Dillon AK, Sciortino CM. Cloning and characterization of a Na^+ driven anion exchanger (NDAE1): a new bicarbonate transporter. J Biol Chem. 2000; 275:24552–24559. [PubMed: 10827195]

Romero MF, Kanai Y, Gunshin H, Hediger MA. Expression cloning using *Xenopus laevis* oocytes. Methods Enzymol. 1998b; 296:17–52. [PubMed: 9779438]

Roos A, Boron WF. Intracellular pH. Physiol Rev. 1981; 61(2):296–434. [PubMed: 7012859]

Rossi A, Superti-Furga A. Mutations in the diastrophic dysplasia sulfate transporter (DTDST) gene (SLC26A2): 22 novel mutations, mutation review, associated skeletal phenotypes, and diagnostic relevance. Hum Mutat. 2001; 17(3):159–71. [PubMed: 11241838]

Saier MH Jr, Eng BH, Fard S, Garg J, Haggerty DA, Hutchinson WJ, Jack DL, Lai EC, Liu HJ, Nusinew DP, et al. Phylogenetic characterization of novel transport protein families revealed by genome analyses. Biochim Biophys Acta. 1999; 1422(1):1–56. [PubMed: 10082980]

Satoh H, Susaki M, Shukunami C, Iyama K, Negoro T, Hiraki Y. Functional analysis of diastrophic dysplasia sulfate transporter. Its involvement in growth regulation of chondrocytes mediated by sulfated proteoglycans. J Biol Chem. 1998; 273(20):12307–15. [PubMed: 9575183]

Sciortino CM, Romero MF. Cation and voltage dependence of rat kidney, electrogenic Na^+/HCO_3^- cotransporter, rkNBC, expressed *in* oocy*tes*. Am J Physiol. 1999; 277(4 Pt 2):F611–623. [PubMed: 10516286]

Scott DA, Karniski LP. Human pendrin expressed in Xenopus laevis oocytes mediates chloride/formate exchange. Am J Physiol Cell Physiol. 2000; 278(1):C207–C211. [PubMed: 10644529]

Shcheynikov N, Kim KH, Kim KM, Dorwart MR, Ko SB, Goto H, Naruse S, Thomas PJ, Muallem S. Dynamic control of cystic fibrosis transmembrane conductance regulator Cl(−)/HCO3(−) selectivity by external Cl(−). J Biol Chem. 2004; 279(21):21857–65. [PubMed: 15010471]

Shcheynikov N, Ko SB, Zeng W, Choi JY, Dorwart MR, Thomas PJ, Muallem S. Regulatory interaction between CFTR and the SLC26 transporters. Novartis Found Symp. 2006a; 273:177–86. discussion 186–92, 261–4. [PubMed: 17120768]

Shcheynikov N, Wang Y, Park M, Ko SB, Dorwart M, Naruse S, Thomas PJ, Muallem S. Coupling modes and stoichiometry of Cl^-/HCO_3^- exchange by Slc26a3 and Slc26a6. J Gen Physiol. 2006b; 127(5):511–24. [PubMed: 16606687]

Shelden MC, Howitt SM, Price GD. Membrane topology of the cyanobacterial bicarbonate transporter, BicA, a member of the SulP (SLC26A) family. Mol Membr Biol. 2010; 27(1):12–23. [PubMed: 19951076]

Sheppard DN, Welsh MJ. Structure and function of the CFTR chloride channel. Physiol Rev. 1999; 79(1 Suppl):S23–45. [PubMed: 9922375]

Sindic A, Mount DB, Romero MF. Renal physiology of SLC26 anion exchangers. Curr Opin Nephrol Hypertens. 2007; 16(5):484–90. [PubMed: 17693766]

Soleimani M, Greeley T, Petrovic S, Wang Z, Amlal H, Kopp P, Burnham CE. Pendrin: an apical $Cl^-/OH^-/HCO_3^-$ exchanger in the kidney cortex. Am J Physiol Renal Physiol. 2001; 280(2):F356–64. [PubMed: 11208611]

Stauber T, Jentsch TJ. Sorting motifs of the endosomal/lysosomal CLC chloride transporters. J Biol Chem. 2010; 285(45):34537–48. [PubMed: 20817731]

Takahashi H, Yamazaki M, Sasakura N, Watanabe A, Leustek T, Engler JA, Engler G, Van Montagu M, Saito K. Regulation of sulfur assimilation in higher plants: a sulfate transporter induced in sulfate-starved roots plays a central role in Arabidopsis thaliana. Proc Natl Acad Sci U S A. 1997; 94(20):11102–7. [PubMed: 9380766]

Taylor JP, Metcalfe RA, Watson PF, Weetman AP, Trembath RC. Mutations of the PDS gene, encoding pendrin, are associated with protein mislocalization and loss of iodide efflux: implications for thyroid dysfunction in Pendred syndrome. J Clin Endocrinol Metab. 2002; 87(4): 1778–84. [PubMed: 11932316]

Urness LD, Paxton CN, Wang X, Schoenwolf GC, Mansour SL. FGF signaling regulates otic placode induction and refinement by controlling both ectodermal target genes and hindbrain Wnt8a. Dev Biol. 2010; 340(2):595–604. [PubMed: 20171206]

van de Kamp M, Schuurs TA, Vos A, van der Lende TR, Konings WN, Driessen AJ. Sulfur regulation of the sulfate transporter genes sutA and sutB in Penicillium chrysogenum. Appl Environ Microbiol. 2000; 66(10):4536–8. [PubMed: 11010912]

Wall SM. The renal physiology of pendrin (SLC26A4) and its role in hypertension. Novartis Found Symp. 2006; 273:231–9. discussion 239–43, 261–4. [PubMed: 17120771]

Wangemann P, Nakaya K, Wu T, Maganti RJ, Itza EM, Sanneman JD, Harbidge DG, Billings S, Marcus DC. Loss of cochlear $HCO3^-$ secretion causes deafness via endolymphatic acidification and inhibition of Ca2+ reabsorption in a Pendred syndrome mouse model. Am J Physiol Renal Physiol. 2007; 292(5):F1345–53. [PubMed: 17299139]

Xie Q, Welch R, Mercado A, Romero MF, Mount DB. Molecular and functional characterization of the Slc26A6 anion exchanger, functional comparison to Slc26a1. Am J Physiol Renal Physiol. 2002; 283:F826–838. [PubMed: 12217875]

Xu J, Henriksnas J, Barone S, Witte D, Shull GE, Forte JG, Holm L, Soleimani M. SLC26A9 is expressed in gastric surface epithelial cells, mediates Cl^-/HCO_3^- exchange and is inhibited by NH_4+ Am J Physiol Cell Physiol. 2005; 289(2):C493–505. [PubMed: 15800055]

Xu J, Song P, Miller ML, Borgese F, Barone S, Riederer B, Wang Z, Alper SL, Forte JG, Shull GE, et al. Deletion of the chloride transporter Slc26a9 causes loss of tubulovesicles in parietal cells and impairs acid secretion in the stomach. Proc Natl Acad Sci U S A. 2008; 105(46):17955–17960. [PubMed: 19004773]

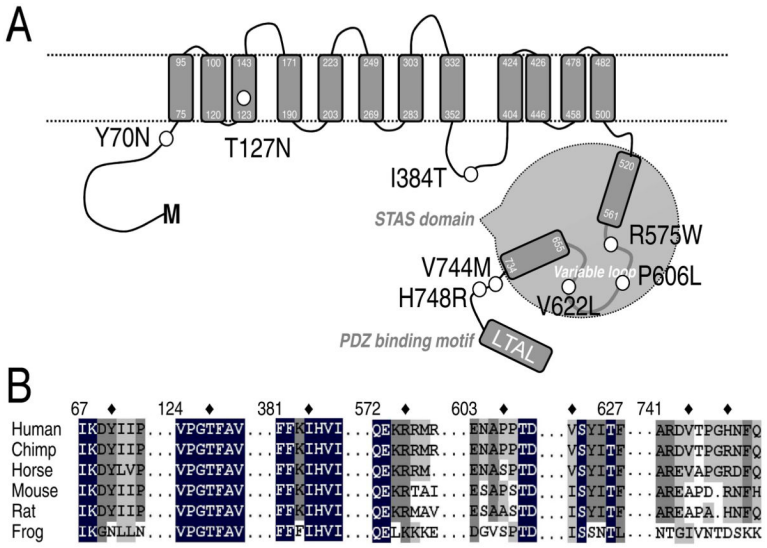

Figure 1. Location and coding residue's conservation of SLC26A9 cSNPs

A. Proposed SLC26A9topology indicating the positions of cSNPs. Transmembrane topology is based on the cyanobacterial bicarbonate transporter, BicA, a member of SulP (SLC26A) family (Shelden, et al., 2010). The border of STAS domain and its variable loop are based on the alignment with SpoIIAA protein and other Slc26 proteins (Aravind and Koonin, 2000; Pasqualetto, et al., 2010). PDZ-binding motif is proposed by(Chang, et al., 2009b). Nonsynonymous cSNPs are indicated by black circles. *B*. Selective alignment of SLC26A9 amino acid sequences 67-73, 124-130, 381-387, 572-578, 603-609, 622-627, 741-751 with corresponding regions of other Slc26a9 proteins. The NCBI/GenBank accession numbers for these sequences are human SLC26A9 (*Homo sapiens* isoform a; NP_443166), chimpanzee Slc26a9 (*Pan troglodytes* isoform 2; XP_514143), horse Slc26a9 (*Equus caballus*; XP_001490875), mouse Slc26a9 (*Mus musculus*; NP_796217), rat Slc26a9 (*Rattus norvegicus*; NP_001100642), frog Slc26a9 (*Xenopus tropicalis*; NP_001096210). The asterisk indicates the coding residue of SLC26A9 cSNPs. The intensity of the shading corresponds to the consensus level of the conserved residues in the gene family.

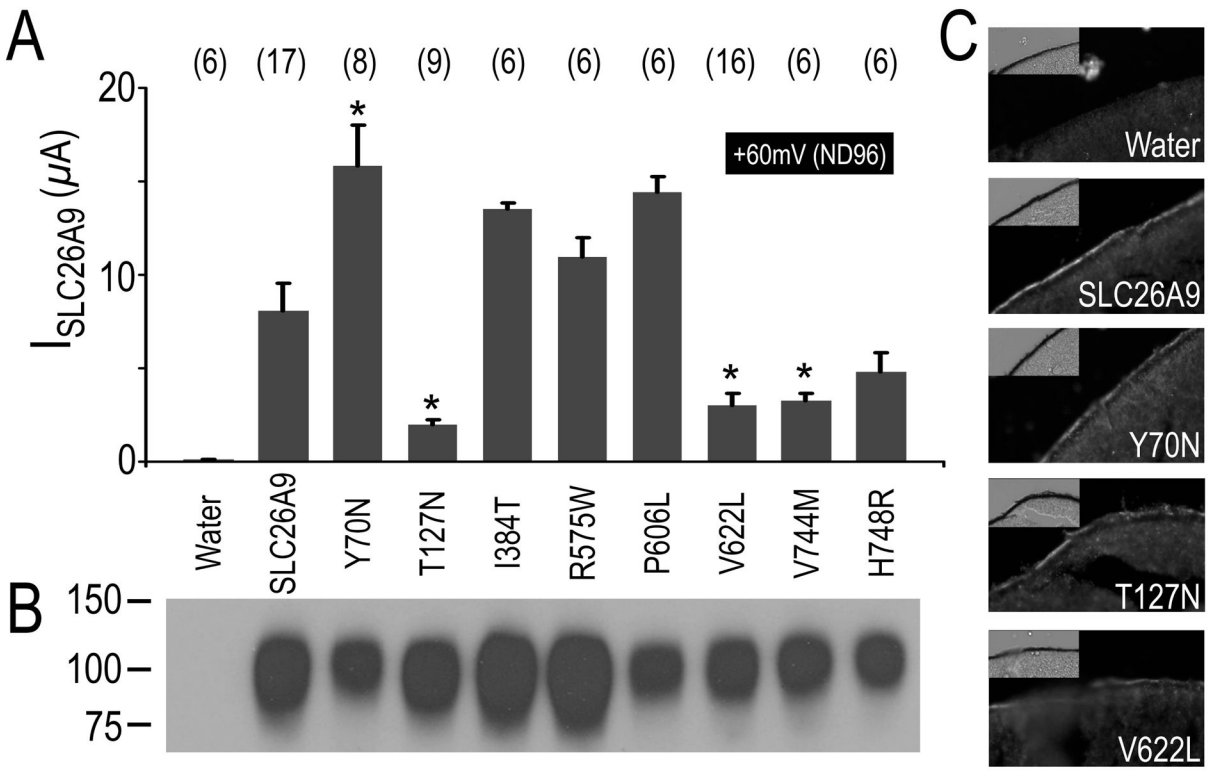

Figure 2. Currents mediated by SLC26A9, cSNPs and surface protein expression

A, Pooled histograms of mean currents at +60mV (ND96 solution) resulting from voltage clamp experiments of Xenopus oocytes injected with cRNAs of SLC26A9 and its eight cSNPs respectively. The number of replications in each group is displayed above each bar as well as (*) indicating statistical difference from SLC26A9 ($P<0.01$). B, Representative western blot of biotinylated proteins (~0.5 oocyte/lane) that were isolated from oocytes expressing triple FLAG-tagged SLC26A9 & cSNPs. And oocytes injecting with water is choose as negative control. Molecular weight markers are displayed to the left of the panel. C, Sections of oocytes injecting with cRNA coding for triple-FLAG tagged SLC26A9 and selective cSNPs (Y70N, T127N and V622L) were labeled with the antibody against the FLAG epitope. Cy3 fluorescence was detected on the membrane of oocytes expressing SLC26A9, Y70N, T127N and V622L, but not water-injected control.

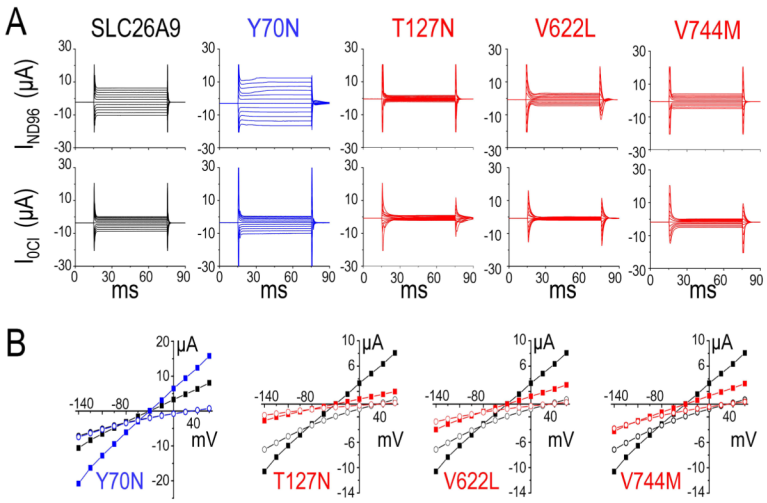

Figure 3.

cSNPs alter Cl^- channel function of SLC26A9.

A. In voltage clamp experiments, current sweeps resulting from the voltage step protocol in ND96 (upper) and a Cl^- free ND96 (lower) for SLC26A9 (black), Y70N (blue), T127N (red), V622L (red) and V744M (red). *B.* Paired comparison of I–V relationships for Y70N (blue), T127N (red), V622L (red), V744M (red) and SLC26A9 (black) respectively. The recordings were made first in ND96 (square) and then in 0 Cl^-/ND96 solution (circle) from *Xenopus* oocytes injected with corresponding cRNAs. The number of experiments for each group is shown in Figure 2A as "(#)".

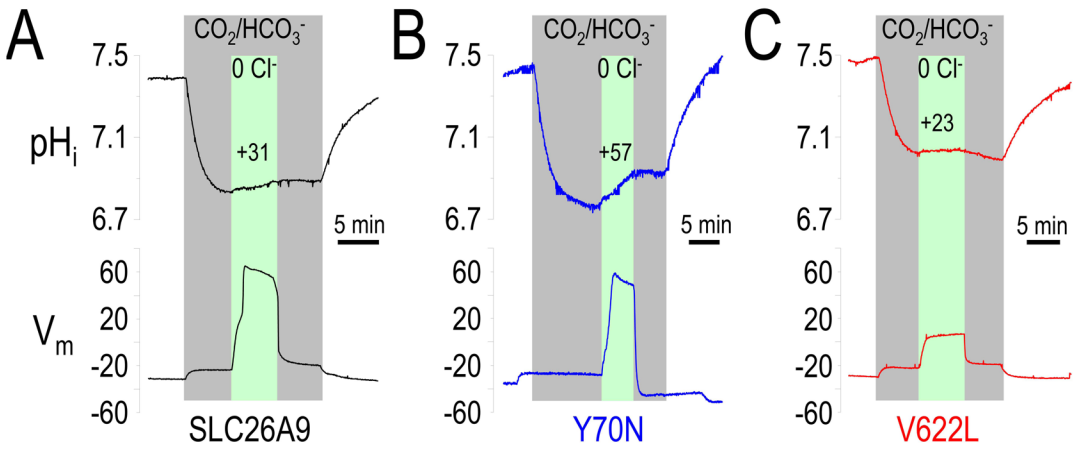

Figure 4. Cl^--HCO_3^- exchanger function of SLC26A9 changed by Y70N and V622L

Representative pH_i experiments for oocytes: SLC26A9 (black, left), Y70N (blue, middle) and V622L (red, right) in 5% CO_2, 33mM HCO_3^- (pH7.5) solution (gray region). Membrane potential (V_m) was measured simultaneously. Extracellular Cl^- removal (0 Cl^-) (green region) depolarized the oocytes and increased pH_i. The average $dpH_i/dt_{(0Cl\text{-}CO2)}$ value ($x10^{-5}$ pH unit/s) reflecting Cl^--HCO_3^- exchange function was displayed above the pH curve during 0 Cl^-/HCO_3^- phrase. Average responses are given in Table 3.

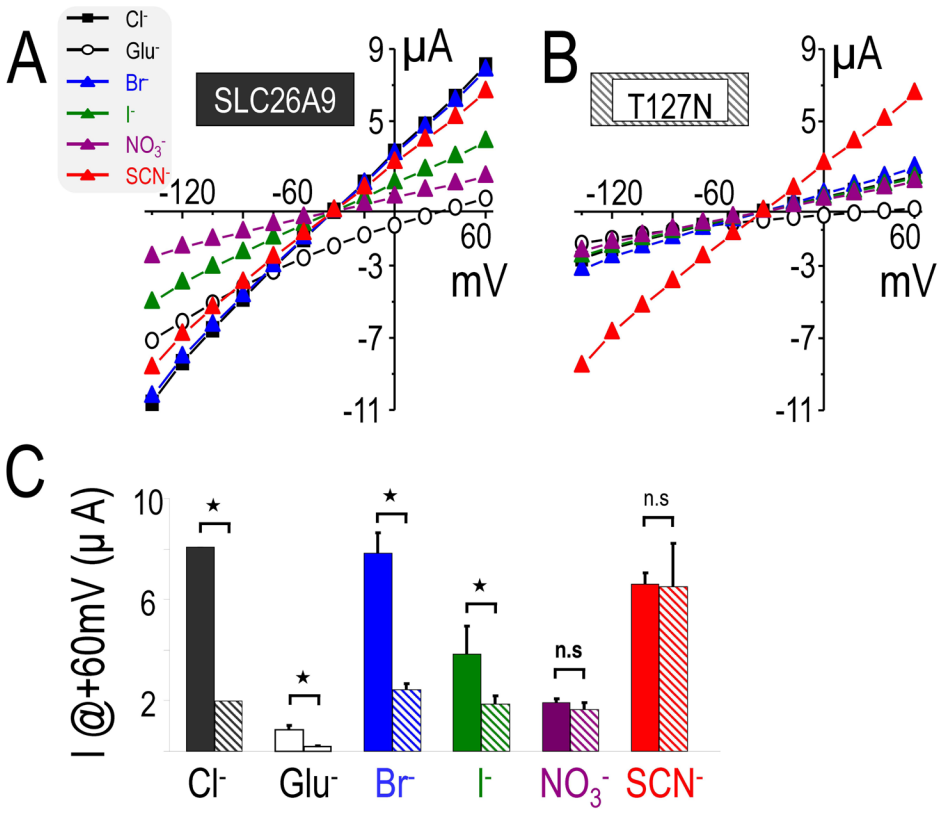

Figure 5. T127N changes the anion conductance order of SLC26A9

A, I–V curve measured from voltage clamp experiments of *Xenopus* oocytes expressing SLC26A9(left) or T127N(right) in ND96 solution containing either 103.6mM Cl^- or 103.6mM of the following anions: gluconate (Glu^-), Br^-, I^-, NO_3^- and SCN^-. B, Pooled histograms of mean currents at +60mV with each of anions (Cl^-, Glu^-, Br^-, I^-, NO_3^- and SCN^-) measured in the oocytes expressing SLC26A9 (left) or T127N (right). "*" indicates significance ($P<0.01$) and "n.s" non-significance between specific pairs of anion substitution experiments.

Hum Mutat. Author manuscript; available in PMC 2013 August 01.

Table 1

Eight non-synonymous, cSNPs of hSLC26A9 in NCBI database [a]

Protein residue	DbSNP rs# Cluster id	Hetero-zygosity	Validation[b]	Minor allele frequency	Primers for mutagenesis
Y70N	rs75021701	0.038	1, 2, 3	0.0312	F: 5′-ccaagtacaagattaaagacaacatcattcctgacctgctc-3′ R: 5′-gagcaggtcaggaatgatgttgtctttaatcttgtacttgg-3′
T127N	rs77497889	0.001	1, 3	N.D[c]	F: 5′-cagatggtgccaggtaactttgccgttatcagc-3′ R: 5′-gctgataacggcaaagttacctggcaccatctg-3′
I384T	rs112659452	0.500	N.D.	N.D.	F: 5′-cagcaacttctttggctccttctttaaaactcatgtcatttgctg-3′ R: 5′-cagcaaatgacatgagttttaaagaaggagccaaagaagttgctg-3′
R575W[d]	rs139697920	0.001	N.D.	N.D.	F: 5′-caagaagcaggagaagtggagaatgaggcccac-3′ R: 5′-gtgggcctcattctccacttctcctgcttcttg-3′
P606L	rs74146719	0.044	1, 2, 3	0.0402	F: 5′-tttgagaatgcgctccccaccgacccc-3′ R: 5′-ggggtcggtggggagcgcattctcaaa-3′
V622L	rs34992672	0.005	1, 2, 3	0.0035	F: 5′-gctaacggcaccagcctgtcctatatcacct-3′ R: 5′-aggtgatataggacaggctggtgccgttagc-3′
V744M	rs3811428	0.008	1, 2, 3	0.0022	F: 5′-ggcaaatgctagagacatgaccccaggacacaa-3′ R: 5′-ttgtgtcctggggtcatgtctctagcatttgcc-3′
H748R	rs16856462	0.196	1, 2, 3	0.0731	F: 5′-cgtgaccccaggacgcaacttccaaggggg-3′ R: 5′-ccccttggaagttgcgtcctggggtcacg-3′

[a]The SLC26A9 cSNPs were collected from NCBI database on 12/7/2010 and were updated on 02/21/2012.

[b]Validation: 1) Validated by multiple, independent submissions to the refSNP cluster. 2) Validated by frenquency or genotype data: minor alleles observed in at least two chromosomes. 3): SNP has been sequenced in 1000Genome project.

[c]N.D. = not determined.

[d]R575W is replaced by R575Q in SLC26A9 cSNPs database (02/21/2012).

Table 2

Experimental solution composition

Standard ND96	**0 Cl^-/gluconate ND96**	**0 Cl^-/Br^- ND96**	**0 Cl^-/I^- ND96**	**0 Cl^-/NO_3^- ND96**	**0 Cl^-/SCN^- ND96**	**Final Conc. (mM)**	**ND96 with 33mM HCO_3^-**	**Final conc. (mM)**
NaCl	Na.gluconate	NaBr	NaI	$NaNO_3$	NaSCN	96	NaCl	63
KCl	K.gluconate	KBr	KI	KNO_3	KSCN	2	KCl	2
$MgCl_2$	$Mg.(gluconate)_2$	$MgBr_2$	MgI_2	$Mg(NO_3)_2.6H_2O$	$Mg.(gluconate)_2$	1	$MgCl_2$	1
$CaCl_2$	$Ca.(gluconate)_2$	$CaBr_2$	CaI_2	$Ca(NO_3)_2.4H_2O$	$Ca(SCN)_2$	1.8	$CaCl_2$	1.8
HEPES	HEPES	HEPES	HEPES	HEPES	HEPES	5.0	HEPES	5.0
							$NaHCO_3$[a]	33
pH	7.5	7.5	7.5	7.5	7.5			7.5
Osm	200±2	200±2	200±2	200±2	200±2			200±2

[a]Before adding $NaHCO_3$, bring solution to 90% volume, and regulate pH to 7.500 by NaOH. Then add 33mM $NaHCO_3$, stir, and bring to 100% volume. Solution was bubbled with 5% CO_2 for 30–40 minutes before experiments.

Table 3

$HCO3^-$ transport properties of SLC26A9, Y70N and V622L

	unit	SLC26A9 (n=6)	Y70N (n=6)	V622L (n=5)
$(dpH_i/dt)_{CO2}$	$\times10^{-5}$ (pH unit/s)	−313 ± 25.4	−289 ± 43.5	−307 ±36.5
$\Delta\ [HCO_3^-]_{CO2}$	mM	5.98 ± 0.78	6.30 ± 0.75	7.19 ± 1.23
$(dpH_i/dt)_{(0Cl\text{-}CO2)}$	$\times10^{-5}$ (pH unit/s)	**+31.3** ± 3.1	**+57.0** ± 12.1	**+23.1** ±4.0
$\Delta\ [HCO_3^-]_{(0Cl\text{-}CO2)}$	mM	**0.79** ± 0.16	**1.94** ± 0.45	**0.40** ± 0.29

Calculations are as indicated under “Methods and Materials”. These data were collected using the two-electrode experiments (pH electrode plus voltage electrode) to *Xenopus* oocytes. The water-injected oocytes show no response to $0Cl^-/HCO3^-/5\%CO_2$ ($Cl^-/HCO3^-$ exchange activity) and its data is as same as previous report (data not shown) (Chang, et.al., 2008). The $dpH_i/dt_{(0Cl\text{-}CO2)}$ values (bold) of Y70N and V622L, the $\Delta\ [HCO_3^-]_{(0Cl\text{-}CO2)}$ value (bold) of Y70N and V622L are significantly different from that of SLC26A9 wild type ($P < 0.05$).